Cell Reports Medicine, Volume *5*

Supplemental information

Age-specific induction of mutant p53 drives clonal hematopoiesis and acute myeloid leukemia in adult mice

Rasoul Pourebrahim, Rafael Heinz Montoya, Hiroki Akiyama, Lauren Ostermann, Shayuan Khazaei, Muharrem Muftuoglu, Natalia Baran, Ran Zhao, Tom Lesluyes, Bin Liu, Joseph D. Khoury, Mihai Gagea, Peter Van Loo, and Michael Andreeff

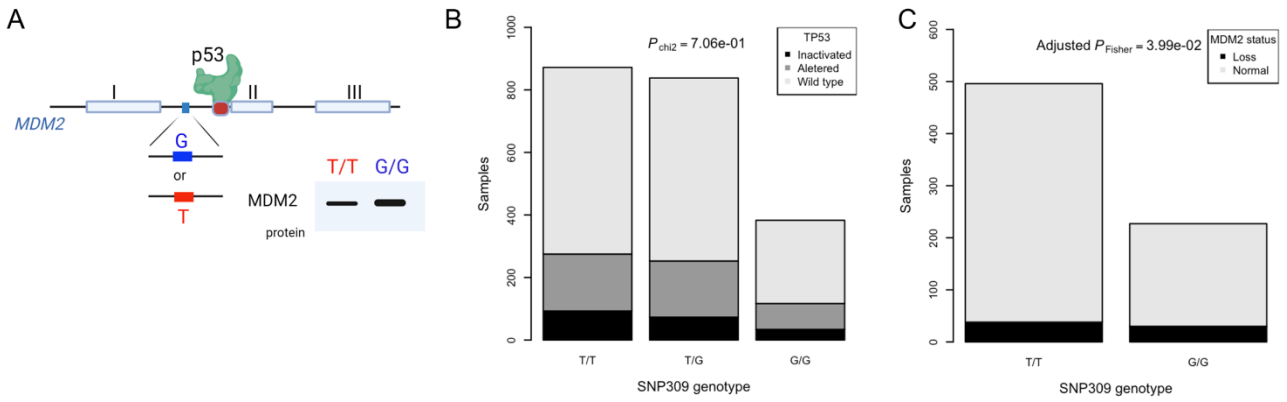

Supplementary Figure S1: *MDM2*^{SNP309} genotype is associated with *TP53* functional status, related to Figure 1. **A**) Schematic representation of *MDM2*^{SNP309} genomic locus and its association with MDM2 levels. The *MDM2*^{SNP309}G allele in the *MDM2* promoter near p53 binding site was shown to increase the levels of *MDM2* RNA and protein. **B**) Barplot of germline *MDM2* SNP309 genotype (T/T, T/G and G/G) depending on somatic *TP53* mutational status (inactivated, altered and wild type). There is no statistical difference amongst those categories (P_{chi2}=0.71). **C**) Barplot of germline *MDM2* ^{SNP309} genotype (T/T versus G/G) depending on *MDM2* copy-number status (loss and normal). This shows a significant difference in G/G cases where *MDM2* losses are more frequent than the ones in T/T cases (adjusted P_{Fisher}=3.99e-2).

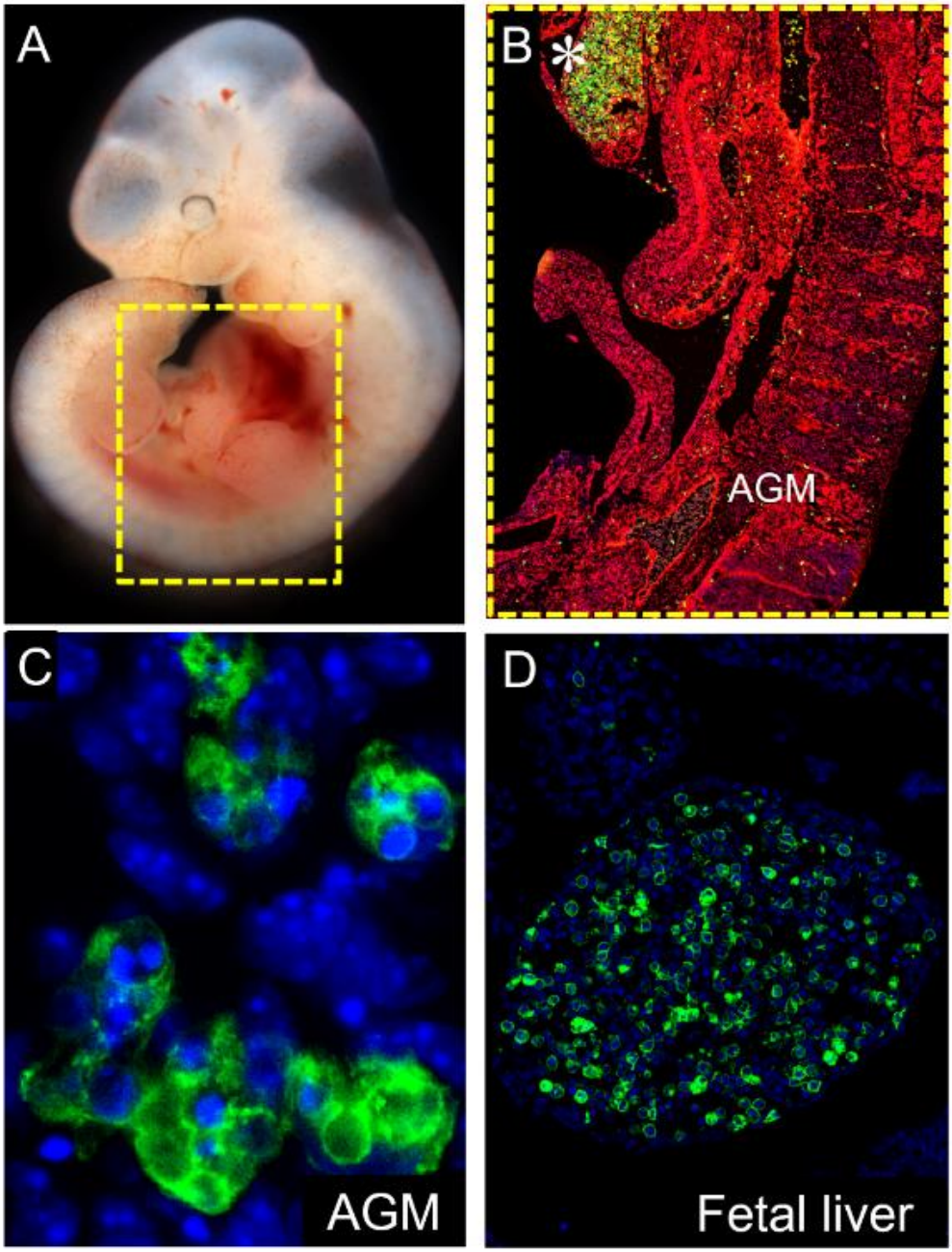

Supplementary Figure S2: *Vav-cre;mTmG* marks early HSCs in the AGM region, related to Figure 2. **A**) Microscopic view of a *Vav-cre;mTmG* mouse embryo at E10.5. The yellow dashed line indicates the AGM region. **B**) Direct fluorescence image of the region marked in panel A, showing the expression of membranous tomato (mT) throughout the whole embryo and membranous GFP (mG) in emerging hematopoietic cells in the AGM and fetal liver (asterisks). **C**) High magnification image of GFP-positive cells in the AGM. **D**) Representative image of GFP-positive cells in the fetal liver.

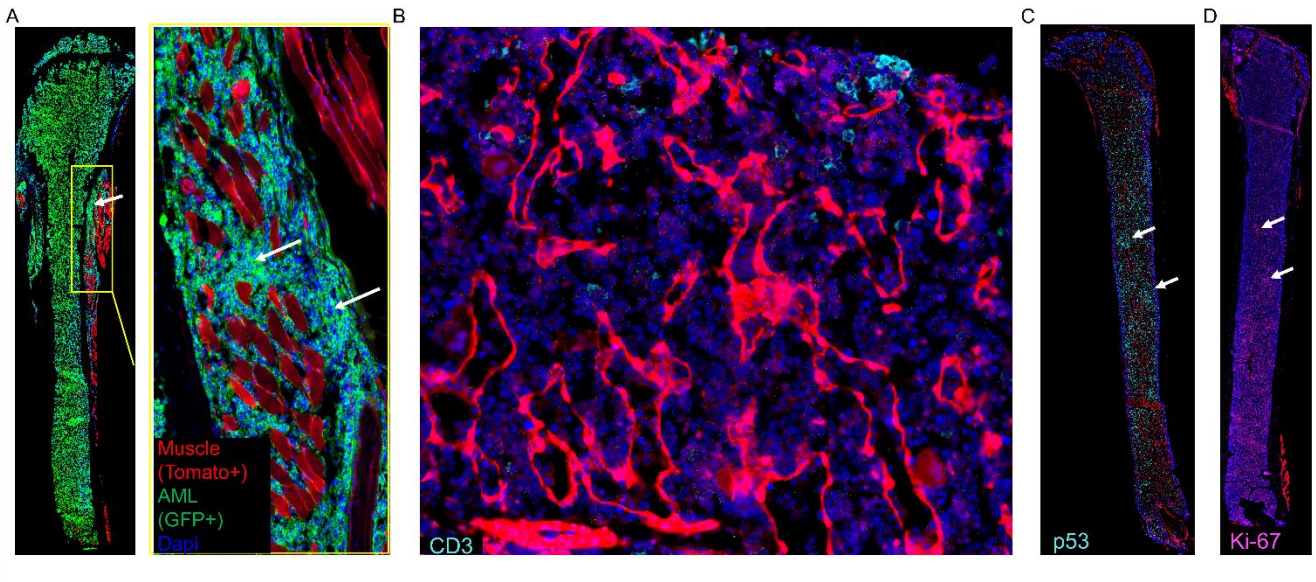

Supplementary Figure S3: Combination of *Mdm2* haploinsufficiency and mutant p53 results in highly proliferative AML, related to Figure 2. **A**) Direct fluorescence image of a longitudinal section of femur isolated from *Vav-Cre;Mdm2*$^{+/fl}$*; Trp53*$^{fl/wmR172H}$*;mTmG* mice with AML, illustrating a hypercellular bone marrow (GFP+) and non-hematopoietic cells (Tomato+). Leukemic cells are observed disrupting the periosteum and invading the muscle compartment (white arrows). **B**) Immunofluorescence image depicting the distribution of CD3+ cells (cyan) within the BM of an AML mouse, showing scattered CD3+ cells with few observed clusters. **C**) Immunofluorescence image illustrating the distribution of p53 mutant-expressing cells (cyan) in a bone marrow section obtained from the mouse mentioned in (A). The red color indicates stromal cells (Tomato+). **D**) Ki-67 expression (magenta) in a parallel section to C, demonstrating the distribution of proliferating cells (Ki-67+) throughout the BM.

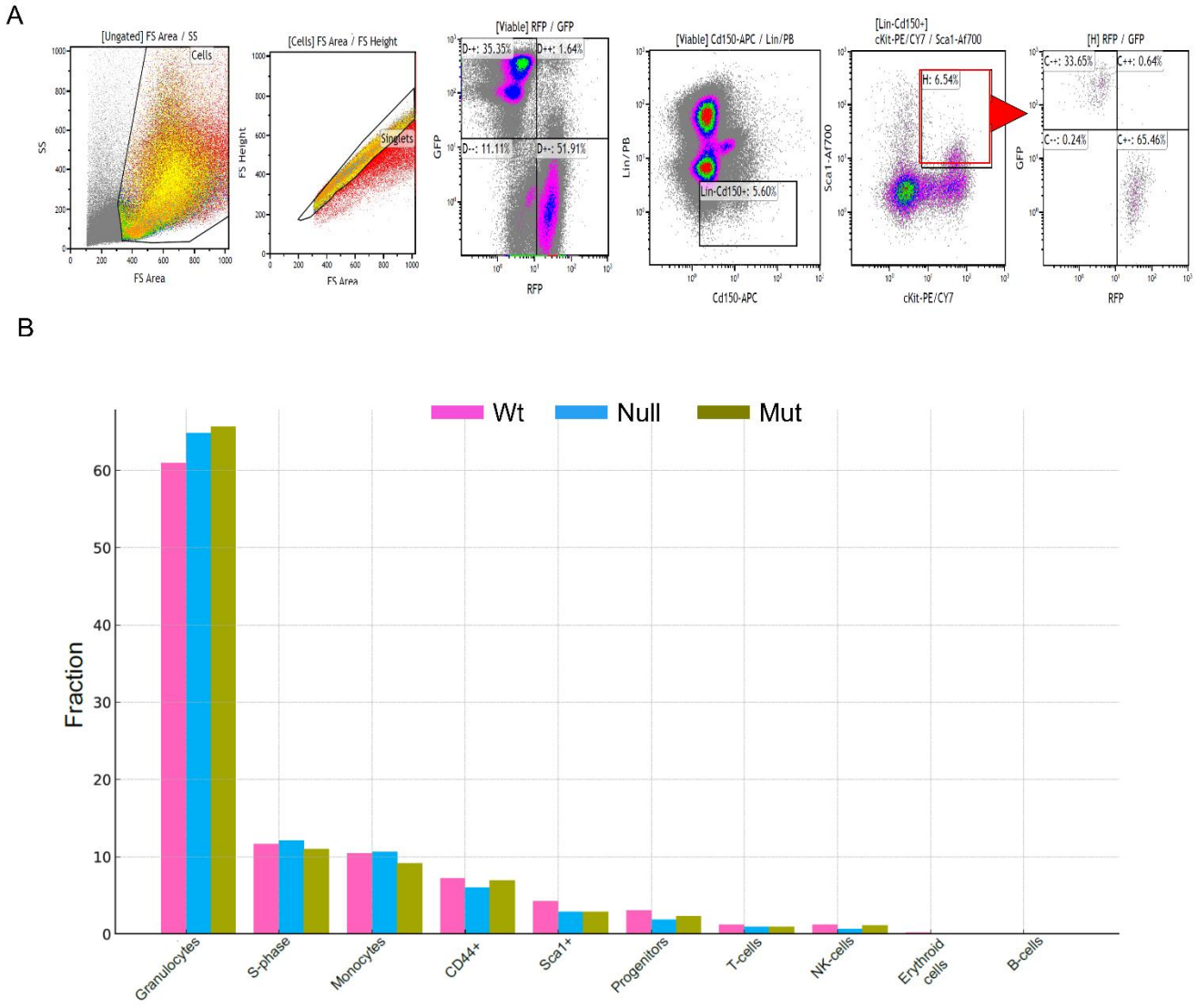

Supplementary Figure S4: Analysis of HSCs targeting and lineage characterization in *Mx1-Cre* mediated recombination and CyTOF profiling, related to Figure 3. **A**) *Mx1-Cre* effectively targets HSCs. A single-cell gate was created based on FSC and SSC parameters to exclude doublets and cell aggregates. To distinguish live cells from dead cells, a live/dead gating step was incorporated. The recombination of *mTmG* allele was confirmed by distinct population of GFP+ and RFP+. The LSK population was identified using a specific gate. LSK cells are characterized by being negative for lineage markers (Lin-) and positive for CD150, Sca-1 and c-Kit markers. After selecting the LSK population, the population of GFP and RFP cells were identified. **B**) Comprehensive characterization of cell lineages using CyTOF analysis in pooled BM samples isolated from *Mx1-Cre;mTmG (*p53 wild-type) ,*Mx1-Cre;Trp53*$^{fl/fl}$*;mTmG (*p53 null), and *Mx1-Cre;Trp53*$^{wmR172H/fl}$*;mTmG (*p53 mutant) mice. The bar plots summarize the subset frequencies in indicated genotypes.

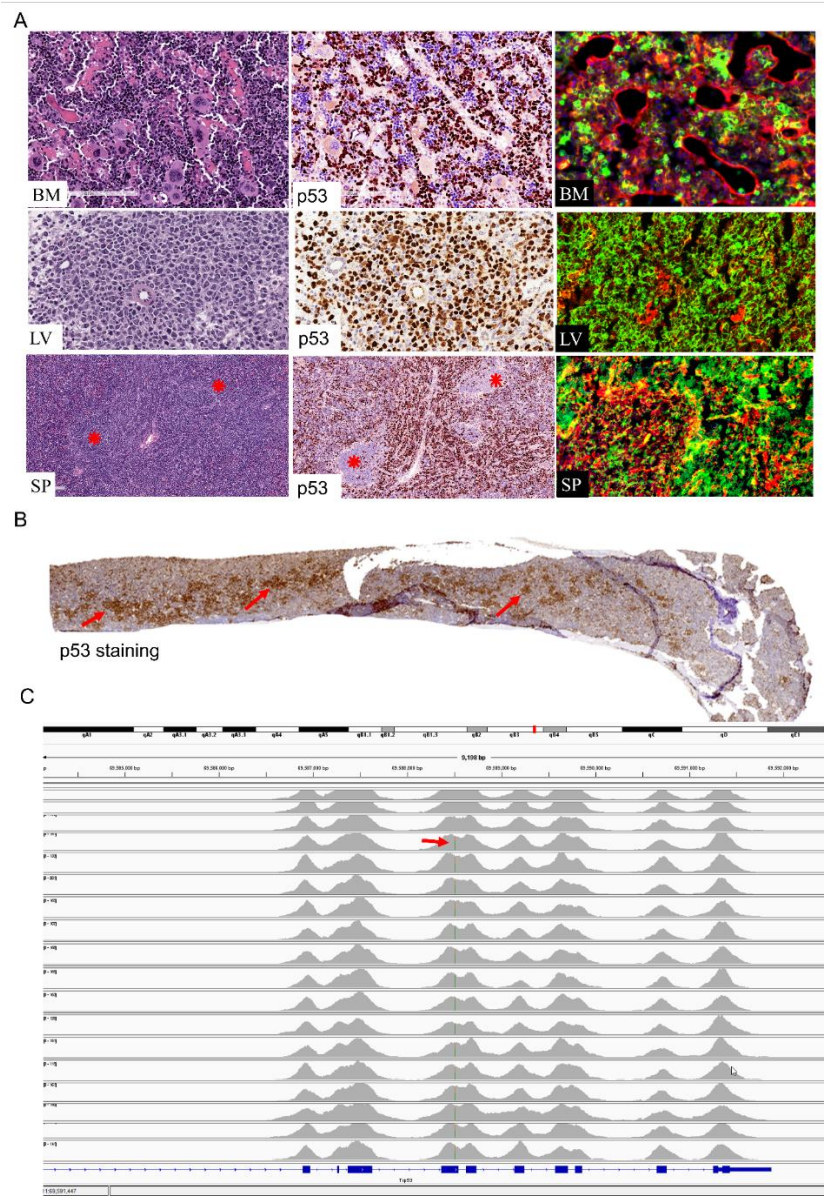

Supplementary Figure S5: Characterization of AML progression and genomic locus *in Mx1-Cre;Trp53*$^{wmR172H/fl}$*;mTmG* mice, related to Figure 4**.** **A**) Histological analysis of bone marrow (BM), liver (LV), and spleen (SP) tissues using hematoxylin and eosin (H&E) staining, revealing infiltration of leukemia cells. Notably, extensive infiltration of leukemia cells is observed in the spleen section, particularly in the periphery of the germinal center (red asterisks). Immunostaining of p53 protein in leukemia cells within BM, SP, and LV tissues is shown (brown staining). Furthermore, direct fluorescence visualization of BM, SP, and LV tissues demonstrates the presence of GFP+ leukemia cells. **B**) Immunostaining of p53 in a longitudinal section of the femur shows the clonal expansion of p53 mutant AML cells (red arrow). **C**) A snapshot of the IGV browser displaying the *Trp53* mutation in AML samples (red arrow).

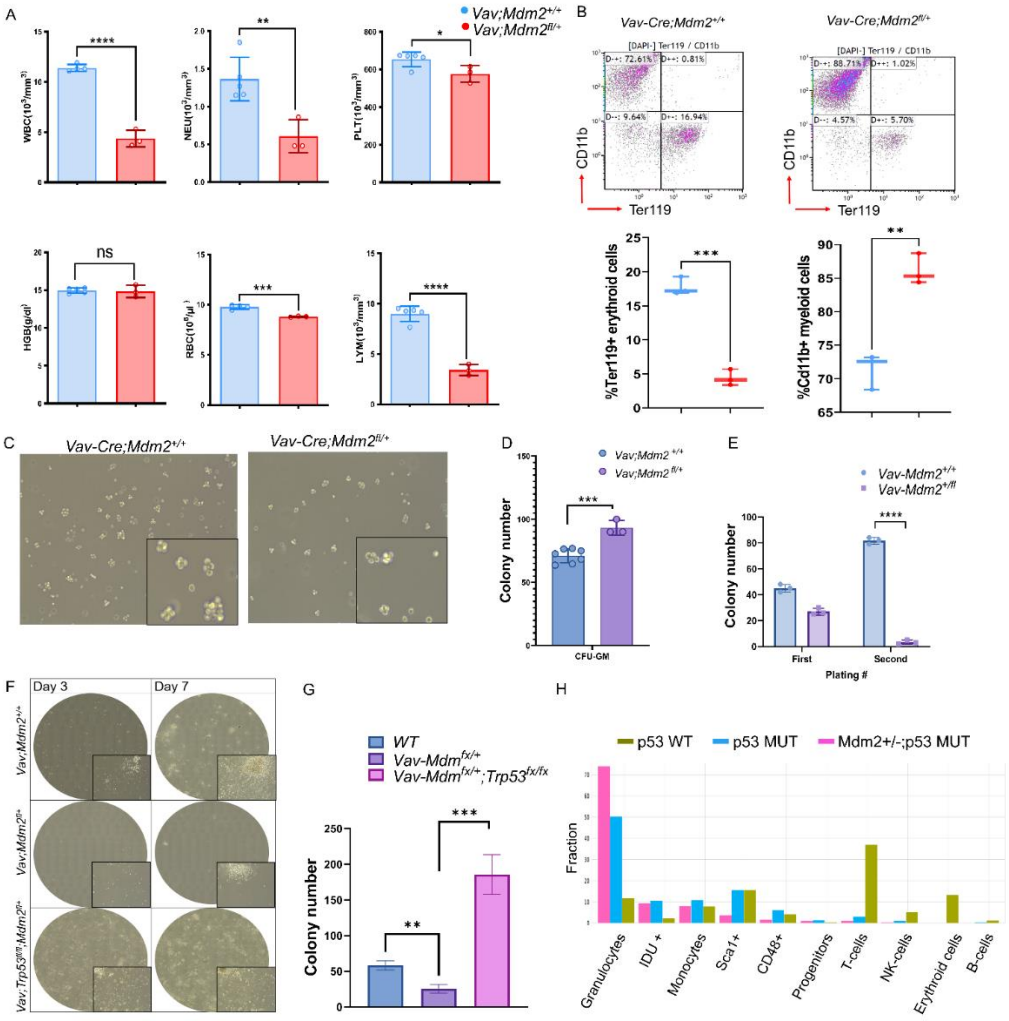

Supplementary Figure S6: Characterization of the hematopoietic phenotype of *Vav-cre;Mdm2*$^{fl/+}$ mice before and after deletion of p53, related to Figure 5. **A**) Peripheral blood indexes in *Vav-cre;Mdm2*$^{fl/+}$. Each plot represents the indicated blood cell type and shows the count values compared to control. Red Blood Cells (RBC), WBC (White Blood Cells), NEU (Neutrophils), LYM (Lymphocytes), PLT (Platelets), HGB (Hemoglobin). ****P < 0.0001, ***P < 0.001, **P < 0.01, *P < 0.5. **B**) Representative flow cytometry plots and quantification of CD11b+ myeloid cells and Ter119+ erythroid cells in CFU cells isolated from the indicated mice. **C**) Representative images of colonies from Vav-cre;Mdm2fl/+ and control mice. The high magnification view is shown in the black box. **D**) Quantification of granulocyte/macrophage colonies (means ± SDs). Each data point represents a measurement from an individual mouse. **E**) Colony number in methylcellulose replating assays using LSK cells from indicated mice. Mean ± SD. Statistical significance indicated by asterisks: ****P < 0.0001, n=3. **F**) Representative images of colonies in indicated mice at indicated time points. **G**) Quantification of colony numbers in (F). ***P < 0.001, **P < 0.01, n=3.

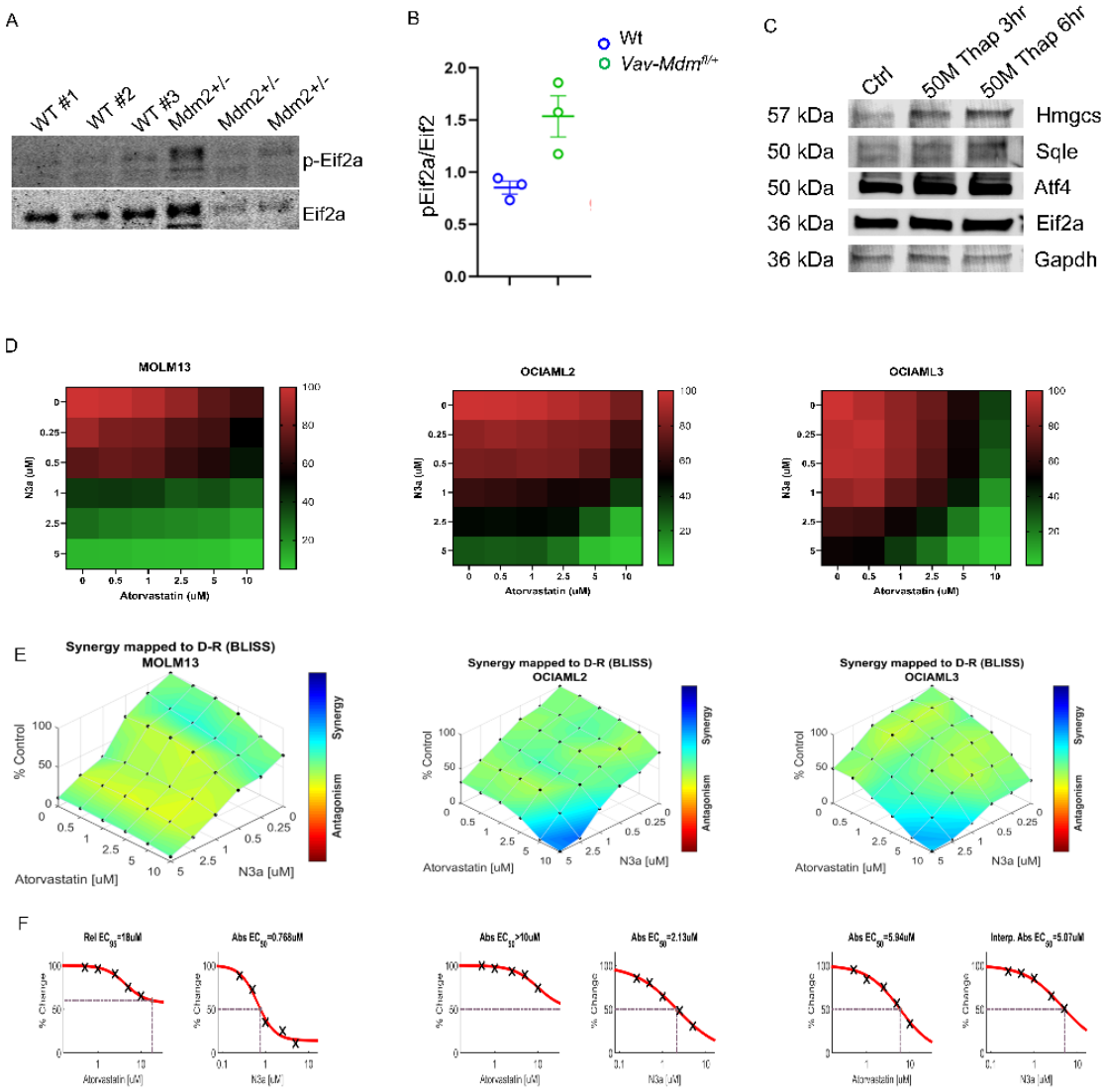

Supplementary Figure S7: ISR activation and therapeutic response assessment, related to Figure 6. **A**) Western blot analysis of phosphorylated eIF2α (p-Eif2a) and total Eif2a levels in BM cells derived from *Vav-Cre;Mdm2*$^{+/+}$ and *Vav-Cre;Mdm2*$^{+/fl}$ mice. **B**) Quantification of protein levels in (A). **C**) Western blot analysis of indicated proteins in K562 cells treated with the ISR activator, Thapsigargin, displaying bands corresponding to the molecular weights of the respective proteins. **D**) Matrix of cell viability under treatment with indicated doses of Atorvastatin (0-10 μM) and Nutlin (0-5 μM) in AML cell lines MOLM13, OCIAML3, and OCIAML2. Each square of the concentration matrix represents a mean value of independent experiments, normalized to levels in DMSO-treated controls, from 3 independent experiments, as measured by CTG assay. **E**) Results of delta BLISS index calculations for AML cell lines using COMBENEFIT software provided by Cancer Research UK Cambridge Institute. **F**) Dose response to single agents and EC50 estimation upon treatment with monotherapy: Atorvastatin and Nutlin. Each data point is expressed as the mean value, with n=3 independent experiments per condition.

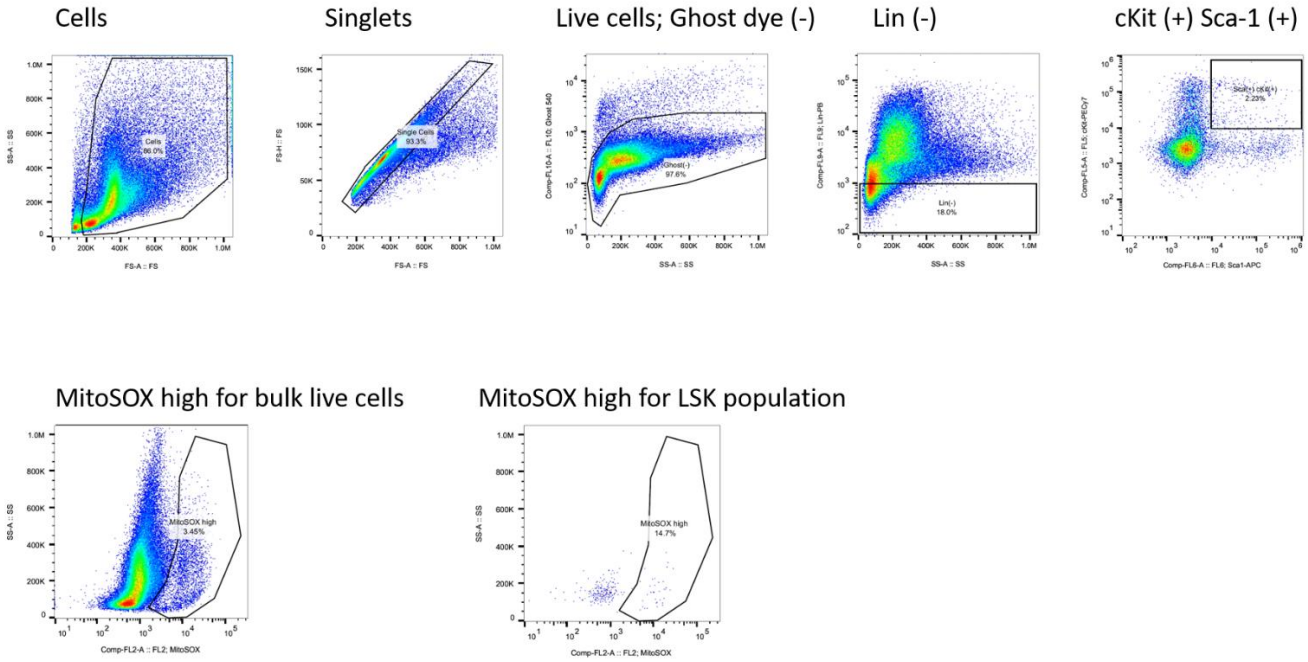

Supplementary Figure S8: Gating strategy for analysis of Mitosox in LSK cells, related to Figure 5. Before proceeding with Mitosox analysis, we applyed appropriate compensation to correct for spectral overlap between fluorochromes used in the experiment. Additionally, appropriate forward scatter (FSC) and side scatter (SSC) parameters were established to exclude debris and other non-cellular events. A single-cell gate was created based on FSC and SSC parameters to exclude doublets and cell aggregates. A live/dead gating step was incorporated to distinguish live cells from dead cells. Next, a gate was applied to identify the LSK population. LSK cells are characterized by being negative for lineage markers (Lin-) and positive for both Sca-1 and c-Kit markers. After selecting the LSK population, a Mitosox gate was applied to identify cells that have taken up the Mitosox dye. Mitosox is a fluorescent dye that accumulates in mitochondria in the presence of superoxide, providing a readout for mitochondrial oxidative stress. The Mitosox gate was set based on fluorescence intensity, comparing the staining with appropriate unstained or negative control cells.

Cre-driver	*Trp53* Status	*Mdm2* Status	Penetrance of Lymphoma	Penetrance of Leukemia
Vav-Cre	Mutant/null ¥	Wt	8/8 (100%)	0/8 (0%)
		Het	3/12 (25%) †	9/12 (75%)
	Null	Wt	7/7 (100%)	0/7 (0%)
		Het	1/7 (10%)	5/7 (71%)
	Mut/+	Wt	5/5 (100%)§	0/5 (0%)
		Het	0/4 (0%)	2/4 (50%)
Mx1-Cre	Mutant/null	Wt	5/10 (50%)‡	10/10 (100%)
		het	0/12 (0%)	11/12 (91%)
	Null	Wt	3/6 (50%) ‡	6/6(50%)
		Het	0/4 (0%)	3/4 (75%)
	Mut/+ *	Wt	-	-
		Het	-	-

¥ Mice harbored one allele of mutant (mut) and the other allele of *Trp53* floxed (null)
† Lack of recombination of *Mdm2* allele was confirmed by PCR.
‡ Animals exhibited normal thymus size, with a mixed phenotype of leukemia/lymphoma and expansion of lymphocytes in spleen.
§ Indicates a long duration of penetrance.
* No malignancy detected after 18 months of observation.

Supplementary table S1: Effects of *Cre*-driver, *Trp53* type, and *Mdm2* status on leukemia penetrance and subtype frequency, related to Figure 2 and Figure 3. The table illustrates the impact of various variables, including the choice of Cre-driver, p53 type (mutant, het vs. null), and *Mdm2* status, on the penetrance of leukemia and the frequency of each leukemia subtype observed in experimental animals.

Tagged Abs. description	Target	Label	Clone	Source	Cat #
CD4(Ms) 115In	CD4(Ms)	115In	RM4-5	BioLegend	100506
Ly-6G/C 139La	Ly-6G/Ly-6C	139La	RB6-8C5	BioLegend	108402
RFP 141Pr	RFP, DsRed	141Pr	Polyclonal	Rockland	600-401-379
CD11c(Ms) 142Nd	CD11c	142Nd	N418	DVS-Fluidigm	3142003B
CD41(Ms) 143Nd	CD41	143Nd	MWReg30	DVS-Fluidigm	3143009B
CD115(Ms) 144Nd	CD115	144Nd	AFS98	DVS-Fluidigm	3144012B
CD8a(Ms) 146Nd (MDA)	CD8a	146Nd	53-6.7	BioLegend	100702
CD19 148Nd (IMC)	CD19	148Nd	D4V4B	CST	90176BF
CD3e 152Sm (MDA)	CD3, CD3e	152Sm	145-2C11	BioLegend	100302
Galectin-3 153Eu	Galectin-3,	153Eu	M3/38	DVS-Fluidigm	3153026B
IFNa(Ms) 154Sm	IFNa	154Sm	RMMA-1	PBL	22100-1
CD34(Ms BM) 156Gd	CD34	156Gd	RAM34	BD	553731
CD14(Ms) 158Gd	CD14	158Gd	Sa14-2	BioLegend	123302
F4/80 159Tb (MDA)	F4/80	159Tb	BM8	BioLegend	123102
CD44 160Gd	CD44	160Gd	IM7	BioLegend	103002
Ter119 162Dy (MDA)	TER-119	162Dy	TER-119	Tonbo	70-5921-U100
CD36(Ms) 163Dy	CD36	163Dy	HM36	BioLegend	102602
Ly-6A/E 164Dy	Ly-6A/E, Sca-1	164Dy	D7	DVS-Fluidigm	3164005B
IFNg(Ms) 165Ho	IFNg	165Ho	XMG1.2	DVS-Fluidigm	3165003B
p53 165Ho	p53	165Ho	184721	R&D	MAB1355
CD117(Ms) 166Er	CD117, c-kit	166Er	2B8	DVS-Fluidigm	3166004B
CD150(Ms) 167Er	CD150, SLAM	167Er	TC15-12F12.2	DVS-Fluidigm	3167004B
Ki67 168Er	Ki67	168Er	B56	BD	556003
GFP 169Tm	GFP	169Tm	5F12.4	DVS-Fluidigm	3169009B
NK1.1(Ms) 170Er	NK1.1	170Er	PK136	DVS-Fluidigm	3170002B
CD11b 172Yb	CD11b	172Yb	M1/70	DVS-Fluidigm	3172012B
MDM2 173Yb	MDM2	173Yb	HDM2-323	Sigma	M7815
CD48(Ms) 174Yb	CD48	174Yb	HM48-1	BioLegend	103433
CD127(Ms) 175Lu	CD127, IL-7Ra	175Lu	A7R34	DVS-Fluidigm	3175006B
Ly-6C 89Y	Ly-6C	89Y	HK1.4	BioLegend	128002

Supplementary Table S2: Antibody panel for CyTOF analysis, related to Figure 3. A comprehensive list of antibodies used in the CyTOF analysis. Each antibody is listed along with its target antigen, metal conjugate, and catalog number. The panel encompasses a wide range of markers targeting various cellular surface proteins and intracellular signaling molecules, enabling the simultaneous assessment of multiple immune cell subsets and functional states.